Journal of
Engineering Sciences
Faculty of Engineering
Assiut University
JES
مجلة
العلوم الهندسية
كلية الهندسة
جامعة أسيوط
journal homepage: http://jesaun.journals.ekb.eg

Comparative Analysis of Nano-powder Reinforcements on Tribological Properties of AA5754 Composites Fabricated via Friction Stir Processing

Received 28 March 2025; Revised 13 May 2025; Accepted 13 May 2025

Bandar Alzahrani [1]

Keywords
Friction stirs processing; Nanocomposites; AA5754; Nanoceramic powder; Hardness; Wear behavior

Abstract: This study aimed to reveal the influence of different nanoceramic powder additions on the hardness and wear behavior of AA5754-based nanocomposites produced via friction stir processing (FSP). CNTs, SiO_2, and Al_2O_3 nano powders were incorporated into an AA5754 matrix using a blind-hole strategy and FSP with a triangular pin tool geometry. Single and double FSP passes were performed at a constant tool rotation speed of 1660 rpm and a traverse speed of 20 mm/min. The developed nanocomposites were characterized based on their microstructure, microhardness, and wear resistance. The results showed the successful incorporation and dispersion of the nano powders in the AA5754 matrix using a triangular pin geometry. Microhardness improved with all nano powder types, with the CNTs reinforcement showing the highest enhancement after both single- and double-pass FSP. Wear resistance was significantly improved in the nanocomposites, particularly with the addition of CNTs, which was attributed to the enhanced load-bearing capacity, improved thermal and mechanical properties, and solid lubrication mechanism provided by the CNTs. Roughness analysis of the worn surfaces revealed a more uniform wear behavior and reduced mean wear depth in the nanocomposites compared to the unreinforced alloy, with CNTs reinforcement exhibiting the most significant improvement, followed by Al_2O_3 and SiO_2. This study demonstrates the effectiveness of FSP in producing AA5754-based nanocomposites with enhanced hardness and wear resistance, highlighting the potential of CNTS reinforcement for superior tribological performance.

1. Introduction

Friction stir processing (FSP) is an emerging metalworking technique (derived from friction stir welding principles) that provides localized adjustment and control of the microstructures in the near-surface layers of processed metallic components [1–3]. It is a novel solid-state technique for fabricating composites without melting the processed material. FSP selectively modifies the microstructure in specific areas to improve mechanical properties, which can be

[1] Mechanical Engineering Department, College of Engineering at Al-Kharj, Prince Sattam Bin Abdulaziz University, Al-Kharj 11942, Saudi Arabia. ba.alzahrani@psau.edu.sa

https://doi.org/10.21608/jesaun.2025.370508.1465

controlled by selecting appropriate tool design and FSP parameters [4–6]. Currently, FSP is a promising technique for fabricating surface composites by dispersing reinforcing particles into a metal matrix and modifying the microstructural features. In FSP, a simple tool with a pin and shoulder is plunged into a metal plate and rotated at a high speed to provide heating and plastic deformation. The heated material softens and flows around the rotating pin [7–9]. The tool is then traversed, forming the processed zone, resulting in a modified microstructure with a fine, equiaxed grain structure [10–12]. Many studies have been dedicated to surface composite fabrication using FSP during this decade to study different mechanical characteristics or to improve the particular mechanical behavior of the composite surface. Alidokht et al. [13] fabricated Al 5083/SiC composite confirmed the increase in hardness. Moreover, they reported that half volume loss in the wear test of the formed using FSP compared to the parent metal. The enhancement in hardness and wear resistance was ascribed to the fine dispersion of the reinforcement particles in the matrix and grain refinement of the matrix. Rana et al.[14] investigated the fabrication of Al 7075-T651- B4C surface composite for various combinations of tool rotation, tool travel speed, and number of passes. They reported that the average hardness of the Al7075/B4C composite fabricated using FSP was 1.3–1.6 times that of the base metal. The wear resistance of the sample processed at the lowest traveling speed was observed to be the highest, despite having the highest coefficient of friction of 0.6. This result was attributed to the higher distribution of B4C particles and the grain strengthening mechanism. Cartigueyen et al.[15] confirmed that the FSP technique has been successfully employed to prepare copper-based surface-level nanocomposites reinforced with nanosized silicon carbide particles (SiCp). The effects of FSP parameters, such as tool rotational speed, traveling speed, and tool tilt angle, on the microstructure and microhardness were investigated. They concluded that the hardness of the nanocomposites was enhanced by decreasing the rotational speed and increasing the traveling speed. The hardness can also be considerably enhanced by increasing the tool tilt angle owing to the good forging/compaction during FSP. Reddy et al. [16] fabricated a B4C-reinforced composite coating on the surface of a Ti-6Al-4V alloy plate through FSP. The wear resistance improved by over 134 times compared with that of the base metal, and the hardness of the composite was doubled. Ranjit et al.[17] investigated AA5083 by incorporating tungsten particles into a matrix using FSP. The composite surface resulted in a uniform dispersion of tungsten particles with excellent interfacial bonding and without the formation of any harmful intermetallic. Moreover, the particles penetrated to a depth equal to the full pin length of the tool. The fabricated 5083 Al–W composite exhibited an improved UTS of more than 100 MPa, with a high ductility (30%). Sharifitabar et al.[18] studied the effect of multipass on the grain refinement and wear resistance of aluminum (Al) alloy 5052- H32 incorporated with Al_2O_3 powder. They observed that grain size refinement with multiple passes was more effective. The hardness of the parent Al alloy was enhanced by almost three times. Moreover, the wear resistance was significantly improved two to three times in the Al/ Al_2O_3 surface nanocomposite layer compared to that of the as-received Al. Zarghani et al.[19] used Al alloy 6082 and incorporated Al_2O_3 powder into it. The surface composite layer produced by the three FSP passes showed better dispersion of Al_2O_3 particles. The hardness of the fabricated composite was higher than that of the parent alloy. The wear resistance was largely improved (two to three times) in the Al/

Al_2O_3 surface nanocomposite layer produced by four FSP passes compared with that in the as-received Al. Wang et al. [20] investigated the effects of incorporating SiC powder in 5A06Al alloy. They reported that the microhardness was steady and 10% higher than that of the base metal owing to the integral dispersed SiC. In another study conducted by Ke et al.[21], the incorporation of Ni powder into a pure aluminum plate was investigated. They concluded that after the 3-pass FSP, the grain refinement and precipitation hardening effect of the Al3Ni intermetallic resulted in a significant increase in the microhardness and tensile strength of the Al– Al3Ni composites.

Based on the above-mentioned review, there is still a need to utilize and optimize different pin shapes to disperse different nanoceramic reinforcements in an Al matrix to fabricate composites and evaluate them in terms of their hardness and wear behavior. Thus, the current study aims to investigate the influence of different nanoceramic powder additions of CNTs, SiO_2, and Al_2O_3 on the hardness and wear behavior of AA5754-based nanocomposites produced via FSP. This study encompasses the evaluation of a blind hole strategy for nano powder incorporation, the effectiveness of triangular pin geometry, the impact of single versus double FSP passes, and the relative performance of each nano powder type as a reinforcement material.

2. Experimental Work

In this study, Al alloy AA5754 sheets with dimensions of 1220 mm × 2440 mm × 10 mm were procured and subsequently sectioned into smaller experimental specimens measuring 100 mm × 200 mm × 10 mm for friction stir processing (FSP). The chemical composition presented in Table 1 and the mechanical properties summarized in Table 2 are based on the mill certificate provided by the supplier (SHAABAN Steel Company Ltd., Riyadh, Saudi Arabia).

Table 1. Chemical composition of the AA5754 initial sheet

Element	Si	Fe	Cu	Mn	Mg	Cr	Zn	Ti	Al
(wt. %)	0.29	0.25	0.0009	0.2432	3.0337	0.0704	0.001	0.0145	Balance

Table 2. Mechanical properties of the AA 5754 initial sheet

Property	Ultimate tensile strength	Proof Stress	Elongation	Hardness
Value	219 MPa	110 MPa	22%	62 HB (1000 g load)

Three types of nano powders were selected as reinforcement materials: CNTs, Al_2O_3, and SiO_2. The Al_2O_3 and SiO_2 nano powders had 99.8% purity with an average particle size of 20 nm, whereas the CNTs exhibited 96% purity with an average diameter of 10-30 nm. To facilitate FSP operations, three distinct tool pin geometries were employed: square, triangular, and circular, as illustrated in Figure 1.

2.1. Matrix plate preparation

AA5754 plates (200 mm × 100 mm × 10 mm) were machined with blind holes of 3 mm diameter and 8.5 mm depth in the center region. The holes were evenly distributed with a center-to-center spacing of 7 mm, as shown in Figure 2. This blind hole strategy was selected over groove configurations because it provides a better initial homogeneous distribution of nano powders across the processed zone. After machining the blind holes, they were carefully filled with the respective nano powders of CNTs, SiO_2, and Al_2O_3, as shown in Figure 2. For each composite specimen, the respective nano powder was incorporated at a volume fraction of 20%, which was calculated based on the total volume of the processed zone.

2.2. Friction stirs processing.

The FSP experiments were conducted using a vertical milling machine equipped with a specialized clamping system that secured the AA5754 plates to a backing plate made of mild steel, as shown in Figure 3a. The FSP was performed in two sequential steps. In the first step, a pinless tool (shoulder only) was fixed to the milling machine and rotated at 1660 rpm.

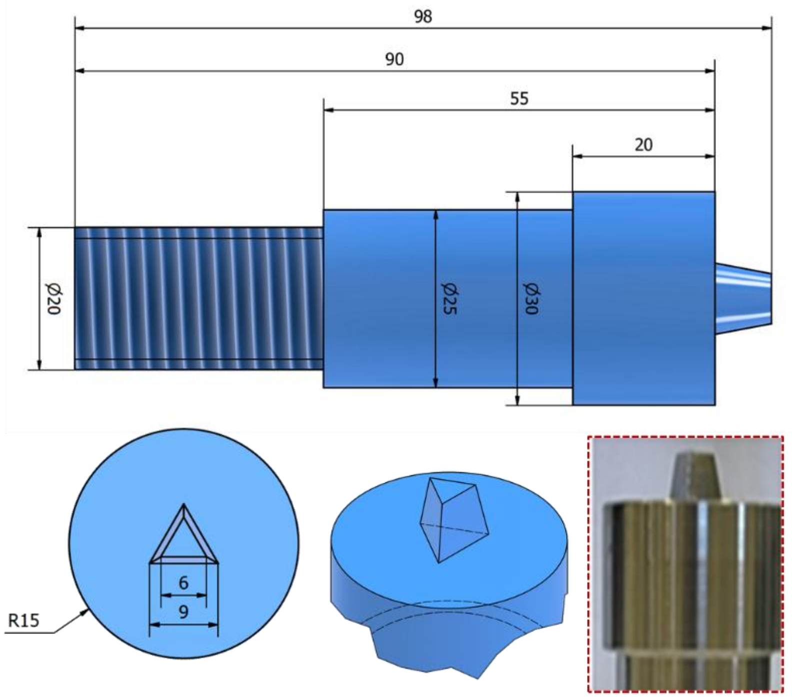

Fig. 1: FSP tool dimensions of tapered pin geometries with triangular pin profile.

This tool was plunged to a shallow depth of less than 0.5 mm on the plate surface and traversed along the hole line at a travel speed of 20 mm/min. This preliminary pass caused the Al to soften and effectively sealed the powder-filled holes, as illustrated in Figure 3b, preventing powder loss during the subsequent processing steps. (2) In the second step, an FSP tool with the appropriate pin geometry (square, triangular, or circular) was mounted on the milling machine. The tool was rotated at 1660 rpm and plunged into the previously sealed line of holes until the shoulder made full contact with the workpiece surface. The tool then traversed along the FSP line at a rate of 20 mm/min, as shown in Figure 3c. For the specimens requiring multiple passes, the process was repeated along the same processing line. Figure 3d shows the AA5754/Al_2O_3 nanocomposite surfaces after single-pass and double-pass FSP operations.

The processing parameters utilized in this study are comprehensively documented in Table 3, which details the combinations of tool shapes, nano powder types, number of passes, travel speed, rotation speed, and tool tilt angle for all nine experimental configurations. Specimen 9 represents the as-received AA5754 material and serves as the control sample for comparative analysis.

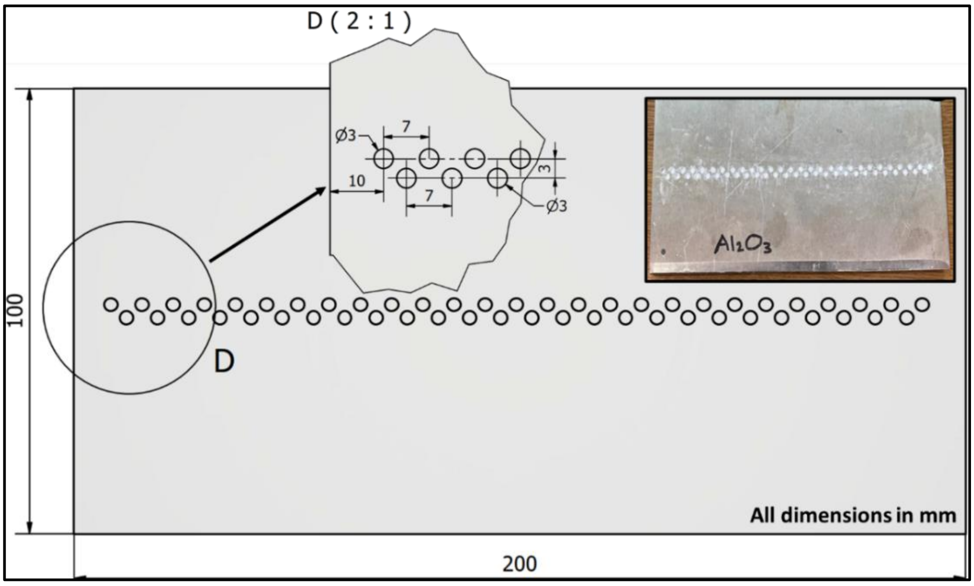

Fig. 2: Dimensions and distribution of the blind holes on the top surface of AA5754.

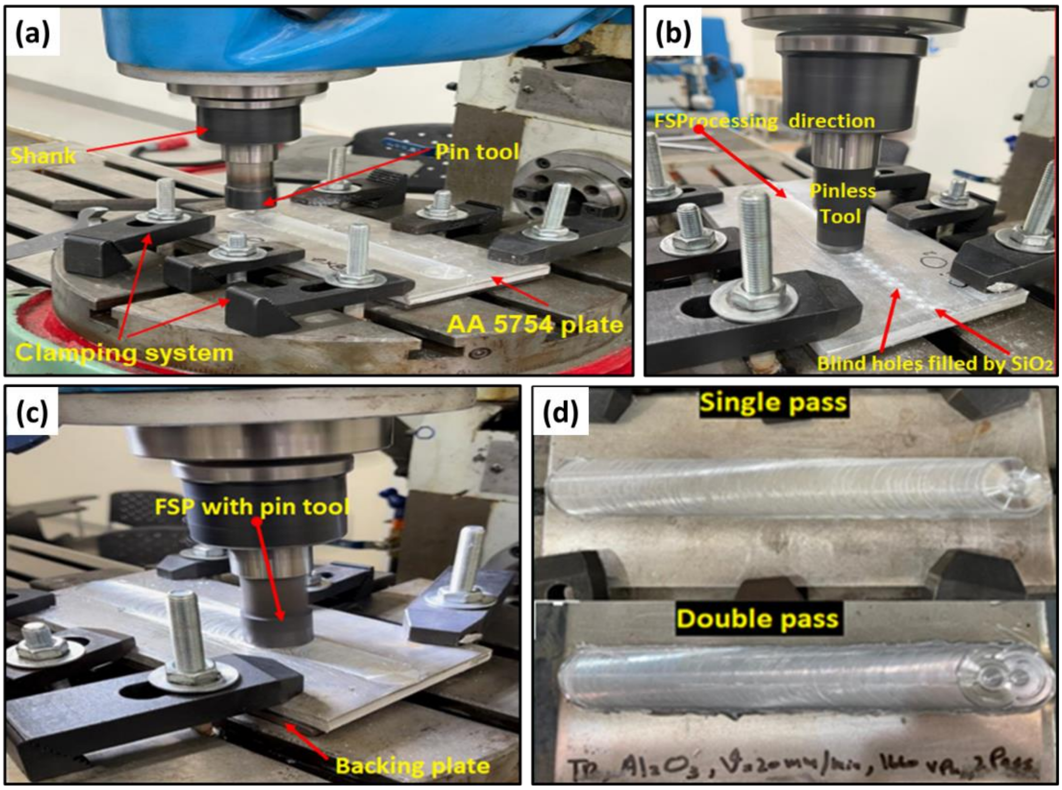

Fig. 3: (a) Image of FSP of AA5754 and fixation setup, (b) initial hole closure using pinless tool, (c) multipass FSP using pin tool, and (d) single-pass and double-pass FSPed AA5754/Al_2O_3 particles.

2.3. Characterization

Following the FSP operations, specimens were extracted from specific locations for microstructural examination, hardness evaluation and wear testing. Figure 4 shows the sampling positions and dimensions of the test specimens. For metallographic examination and hardness assessment, transverse cross-sections (Figure 4a) were prepared according to standard metallographic procedures. This involved sequential grinding with emery papers of increasing fineness up to 2000 grit, followed by mechanical polishing using alumina suspension, initially with 6 µm and subsequently with 1 µm particles. The polished specimens were etched for 40 s in a solution containing 100 ml distilled water, 5 ml HNO_3, 3 ml HCl, and 2 ml HF. After etching, the samples were thoroughly cleaned with acetone and dried before microstructural analysis using an Olympus optical microscope. Vickers microhardness measurements were performed using a digital hardness tester (model HVS-1000) in accordance with the ASTM E92-82 standard, applying a load of 1000 g. The indentations were systematically distributed across the composite regions to obtain comprehensive hardness profiles, as shown in Figure 4a. Wear tests were performed according to the ASTM G99-95 standard. Given the preliminary results indicating the superior performance of triangular pin-shaped tools, wear testing was limited to the specimens processed with this geometry. Specimens for wear testing were prepared with dimensions matching the holder specifications of the pin-on-disk tribometer: cylindrical shape with a diameter of 8 mm and a height of 15 mm (Figure 4b). The testing conditions included a bar load of 7 N, sliding speed of 0.4 m/s, and varied test durations of 5, 10, 15, and 20 min. Each wear test was repeated twice to ensure data reliability and consistency of the results. Figure 4c shows a schematic of the pin-on-disk wear testing setup used in this study. Surface roughness analysis map and wear track depth were conducted using Gwyddion 2.68 software (GNU General Public License version 2.0, GPLv2), a specialized scientific tool for SPM data visualization and analysis. High-resolution SEM micrographs of the worn surfaces were imported into Gwyddion and processed using the Statistical Quantities tool to calculate the roughness parameters.

Table 3. Matrix of the applied FSP parameters

No	Tool pin profile	Powder	Number of Passes	Travel speed (mm/min)	Rotation Speed (rev/min)	Tilt angle	Vol. %
1	Triangle	CNTs	One	20	1660	3º	20
2	Triangle	SiO_2	One	20	1660	3º	20
3	Triangle	Al_2O_3	One	20	1660	3º	20
4	Triangle	Without	One	20	1660	3º	20
5	Triangle	CNTS	Two	20	1660	3º	20
6	Triangle	SiO_2	Two	20	1660	3º	20
7	Triangle	Al_2O_3	Two	20	1660	3º	20
8	Triangle	Without	Two	20	1660	3º	20
9	As received						

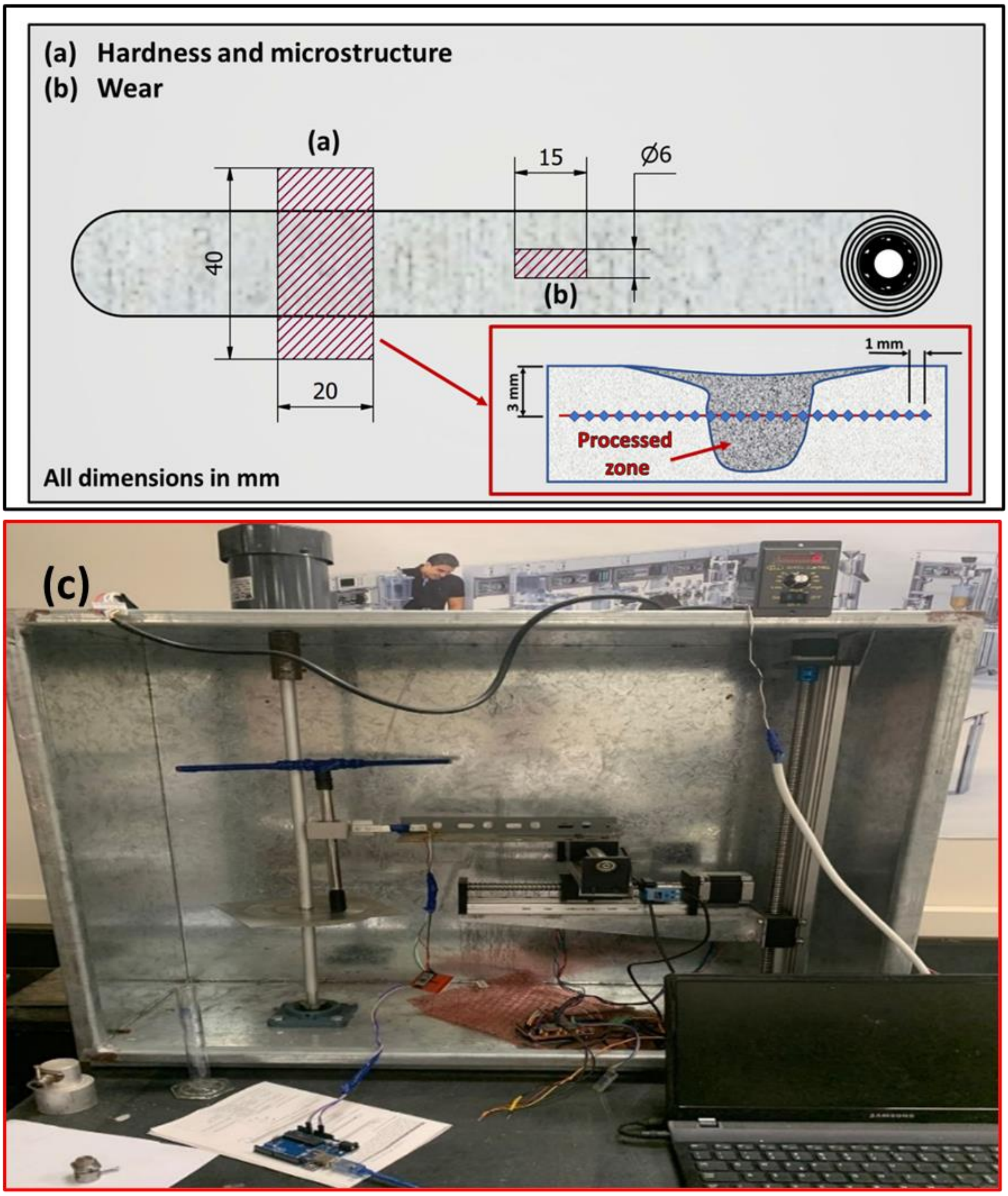

Fig. 4: Sketch of (a) dimensions of the extracted FSP composite specimens and (b) pin-on-disk wear test system.

3. Results and discussion

3.1. Optical macro and microstructures

The macrographs of the FSPed samples revealed that the single-pass process resulted in almost complete closure of the blind holes filled with nano powders, distributing them across the processed zone (nugget zone). However, macro tunnel defects were observed in the samples containing CNTs and SiO_2 after one pass, as shown in Figures 5c and 5e). These defects can be attributed to several interrelated factors: insufficient forging pressure during the initial pass, which failed to fully consolidate the processed zone; the inherent properties of CNTs and SiO_2 nano powders, which may affect material flow behavior differently than

Al_2O_3; and the high volume fraction (25%) of nano powders used in this study, which required more extensive mixing to achieve complete consolidation. CNTs, in particular, possess high aspect ratios and tend to agglomerate owing to strong van der Waals forces, potentially creating localized regions with different flow characteristics during FSP.

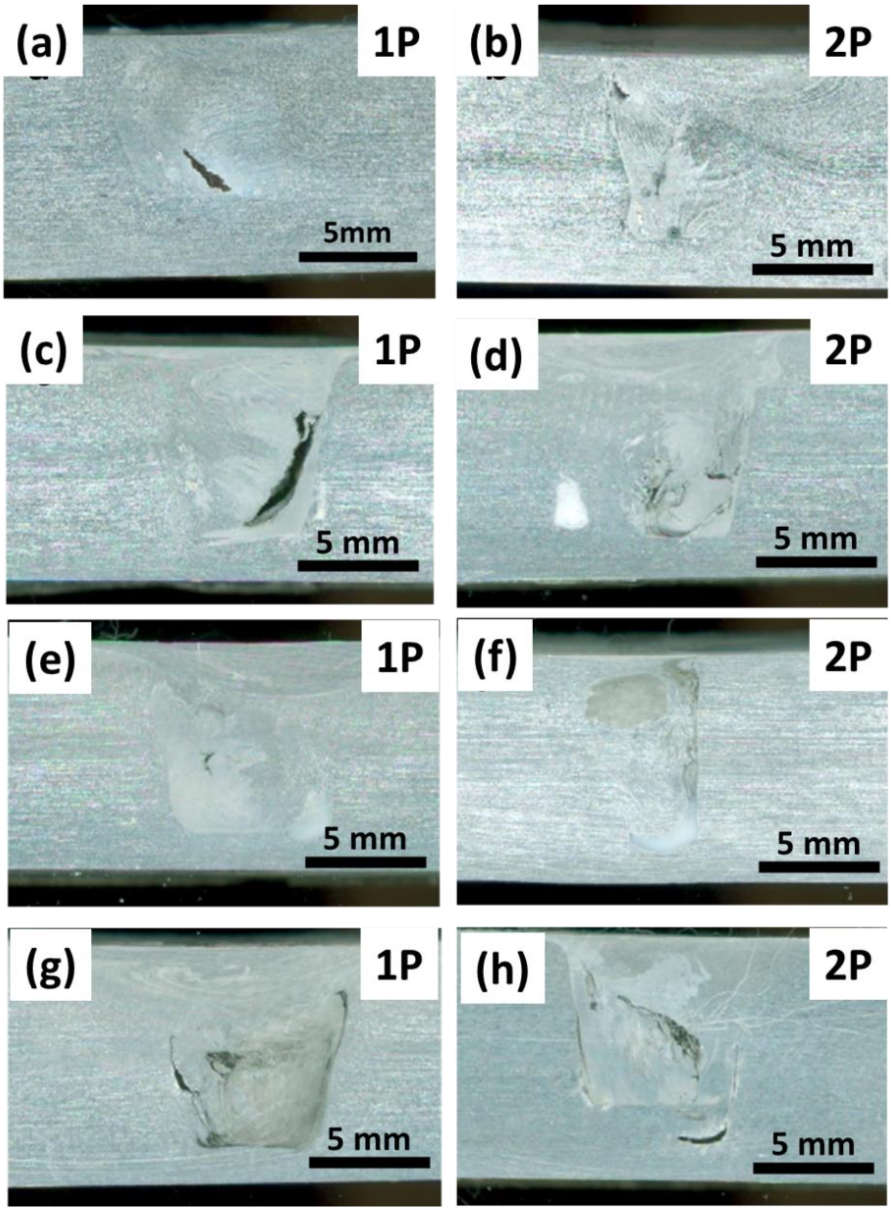

Fig. 5: The transverse cross-section macrograph of AA5754 processed composites: (a,b) AA5754/CNTS, (b,c) AA5754/SiO_2, (e, f) AA5754/ Al_2O_3, and (g,f) unreinforced AA5754.

Similarly, SiO_2 nanoparticles, with their high hardness and relatively low thermal conductivity compared to the aluminum matrix, may create localized thermal gradients that affect material flow and consolidation. These material-specific properties, combined with the processing parameters used in this study, contributed to the formation of the observed macro tunnel defects. In contrast, the two-pass FSP significantly reduced the size of these macro tunnel defects, often eliminating them, as shown in Figures 5b, 5d, and 5f. This improvement suggests that multiple passes enhance the material flow and nano powder dispersion through additional plastic deformation and thermal cycling, resulting in a more uniform microstructure. The second pass effectively provides additional forging pressure and heat input, which helps to close voids and improve particle distribution throughout the matrix [22–24].

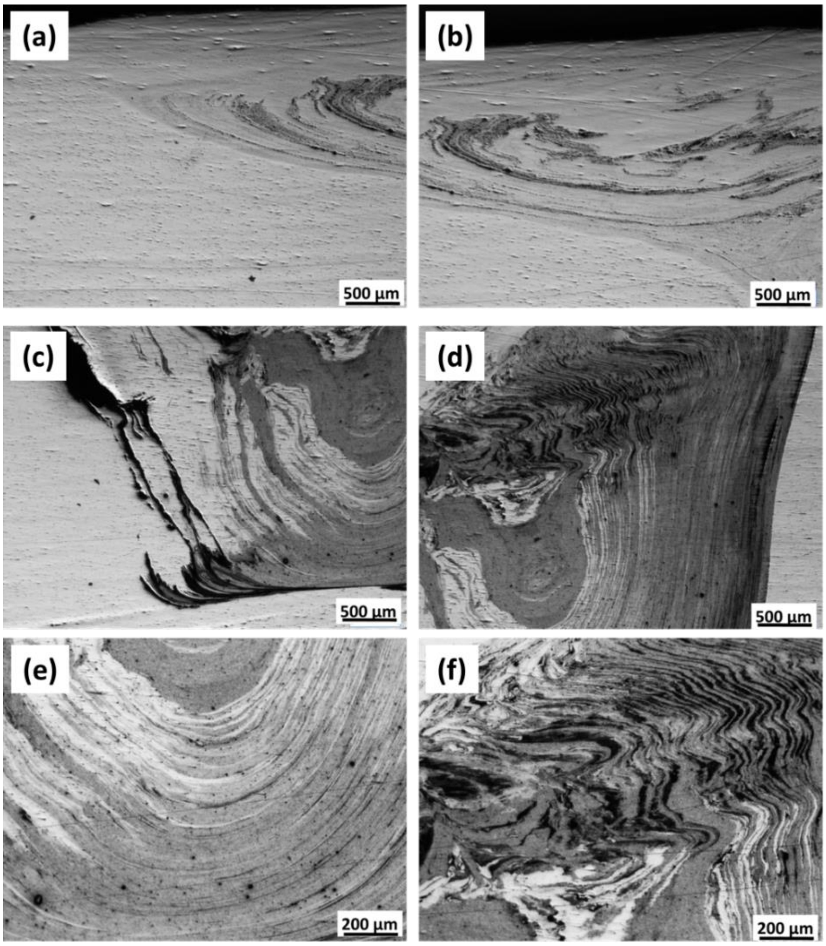

Fig. 6: Microstructure of the AA5457/ CNTS FSPed composite sample after two passes.

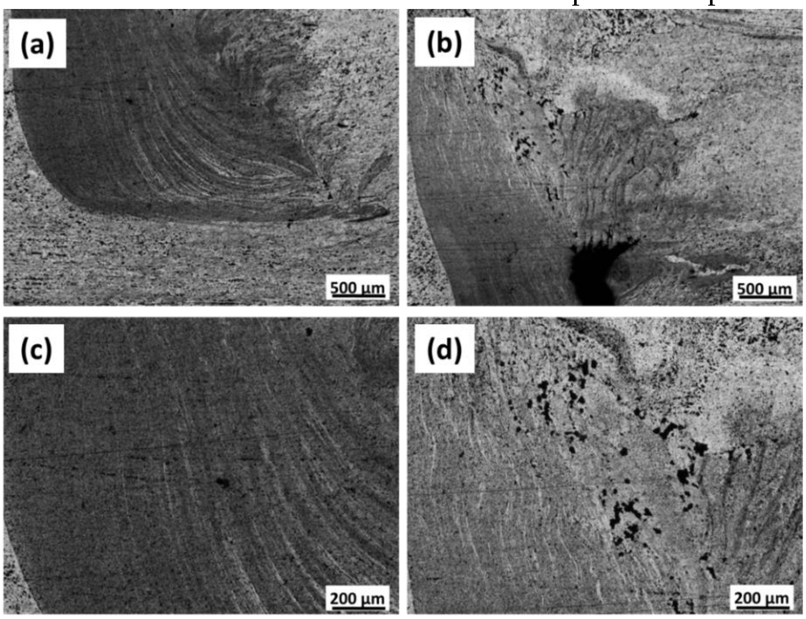

Fig. 7: Microstructure of AA5457/ SiO_2 FSPed composite sample after two passes.

3.2. Hardness profiles

The hardness profiles across the transverse cross-sections of the AA5754 samples processed by FSP and reinforced with CNTs, SiO_2, and Al_2O_3 after one and two passes are presented in Figure 8. For the single-pass FSP specimens (Figure 8a), all the reinforced composites exhibited marked improvements in hardness compared with the unreinforced AA5754, with average hardness values of 71.8, 68.4, and 64.8 HB for the CNTS, SiO_2, and Al_2O_3 reinforcements, respectively, compared with 62.2 HB for the unreinforced specimen. The CNTS-reinforced composite demonstrated the most substantial improvement, with an approximately 15.4% increase compared to that of the base material. This superior hardness can be attributed to the unique properties of CNTs, particularly their exceptional mechanical strength and ability to form strong interfacial bonds with the Al matrix, which effectively impedes dislocation movement during deformation. The SiO_2-reinforced composite exhibited the second-highest hardness improvement with a 10.0% increase, which can be attributed to the hardness of the silica nanoparticles and their relatively uniform dispersion throughout the matrix. The Al_2O_3-reinforced composite demonstrated a modest improvement of 4.2%, which, while still beneficial, was less pronounced than that of the other reinforcements. The implementation of a second FSP pass, as shown in Figure 8b, resulted in further hardness improvements in all the specimens. The average hardness values increased to 75.4, 74.1, and 70.6 HB for the CNTS, SiO_2, and Al_2O_3 reinforcements, respectively, compared with 67.5 HB for the unreinforced specimen. This represents increases of 5.0%, 8.3%, and 9.0% for each reinforcement type compared with their single-pass counterparts. The more substantial percentage improvement observed in the Al_2O_3-reinforced composite after two passes suggests that the second pass was particularly effective in breaking up the agglomerates and achieving better particle distribution. Another notable observation from Figure 8 is the width of the hardened zone, which expanded after the second pass for all the specimens. This widening effect can be directly attributed to the enhanced material flow and more extensive mixing achieved during the multipass processing. The second pass effectively redistributes the nano powders across a broader area while simultaneously refining the grain structure, resulting in a more extensive region with improved mechanical properties. Notably, the hardness profiles exhibited relatively consistent values across the processed zone, with sharp transitions at the boundaries. This pattern indicates good stability of the strengthening mechanisms within the processed region. The consistent hardness plateaus observed, particularly in the CNTs-reinforced specimens, suggest a homogeneous distribution of the reinforcing phase. The overall hardness enhancement can be attributed to several complementary strengthening mechanisms of grain refinement due to dynamic recrystallization during FSP, Orowan strengthening from the nonreinforcements impeding dislocation movement, load transfer between the Al matrix and the stronger reinforcement phases, and generation of geometrically necessary dislocations due to the coefficient of thermal expansion mismatch between the matrix and reinforcements. The results align with previous study by Ostovan and Amanollah [25] investigated the fabrication of Al5083 surface hybrid nanocomposites reinforced by CNTs and Al_2O_3 nanoparticles using FSP. They demonstrated a significant increase in hardness, with the highest value reaching 126 HV in the stirred zone, owing to their superior mechanical properties and ability to form strong interfacial bonds with the matrix, effectively impeding dislocation movement during deformation. Another study by Mirjavadi et al. [26] focused on the effect of multi-pass FSP on the micromultipass and mechanical properties of AA5083/ZrO_2 nanocomposites. They found that multiple passes led to superior hardness and grain refinement, as additional passes promoted better particle dispersion and reduced the agglomeration. El-Sayed et al. [27] investigated the impact of multiple FSP passes on the mechanical properties of SiO_2/5083 Al metal matrix nanocomposites. They fabricated in situ SiO_2/5083 Al nanocomposites using FSP with varying numbers of passes (one to four). The process parameters were set at a rotation speed of 400 rpm and travel speed of 100 mm/min. They demonstrated that a single FSP pass yielded optimal improvements in the mechanical properties. Specifically, the ultimate tensile strength, elongation, microhardness, and impact energy increased by approximately 110.6%, 132.1%, 131.7%, and 125.4%, respectively, compared with those of the BM. These enhancements were attributed to the grain refinement and uniform dispersion of the SiO_2 nanoparticles within the Al matrix.

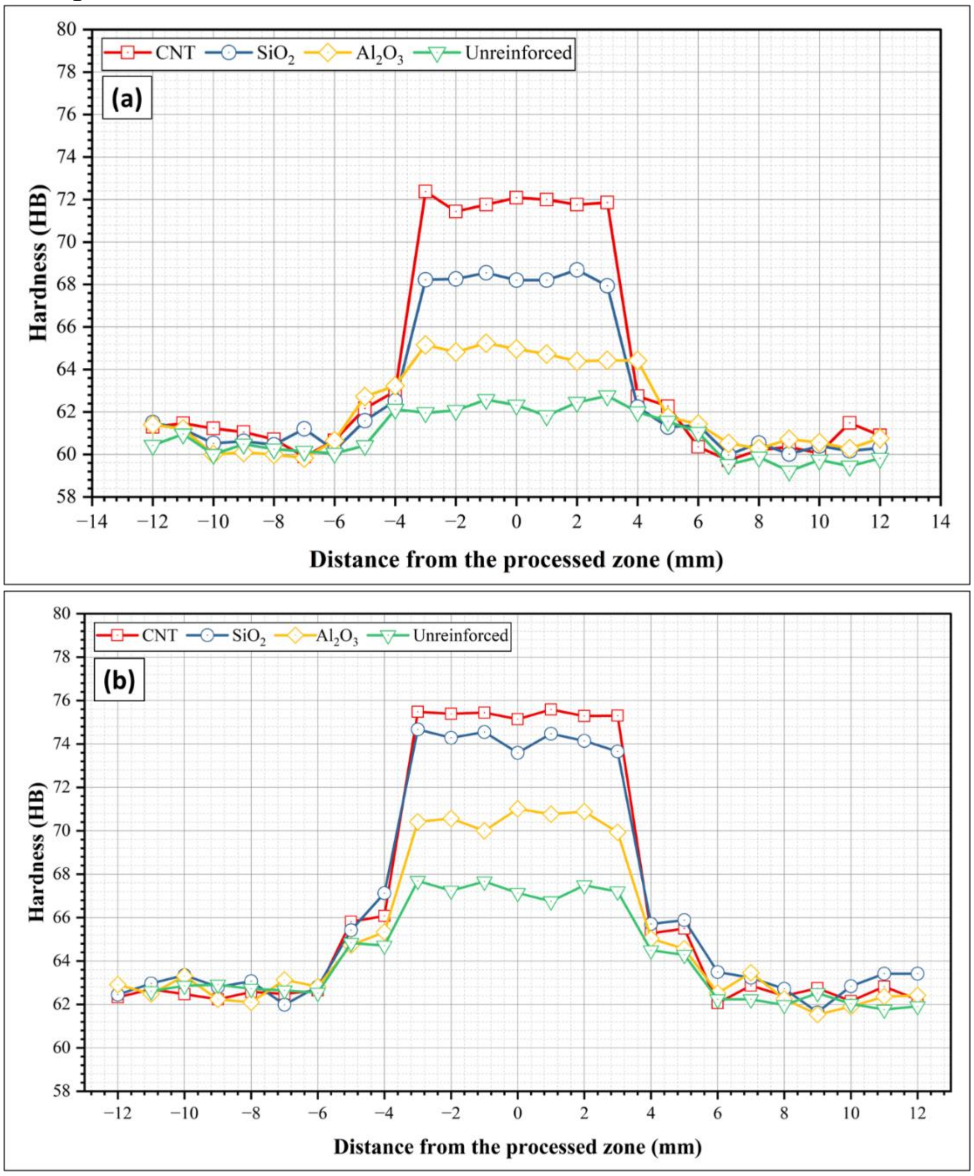

Fig. 8: Hardness profiles across the transverse cross-sections of the AA5457 processed samples reinforced with CNTS, SiO_2, and Al_2O_3 after (a) one pass and (b) two passes.

3.3. Wear Test Results

3.3.1. Wear behaviors of FSPed composites.

The wear behavior of the AA5754 FSPed samples was systematically evaluated through pin-on-disk wear tests under dry conditions with a load of 7 N, a sliding speed of 0.4 m/s, and varying test durations of 5, 10, 15, and 20 min. Figures 9 and 10 show the specific wear rates of the AA5754 FSPed samples processed using one and two passes, respectively. For the single-pass FSPed samples (Figure 9), all reinforced composites exhibited significantly lower specific wear rates than the unreinforced AA5754 material across all testing durations. The CNTS-reinforced composite demonstrated the best wear resistance, with the lowest specific wear rate values of 4.8×10^{-4}, 2.2×10^{-4}, 2.0×10^{-4}, and 2.0×10^{-4} $mm^3/N\cdot m$ at 5, 10, 15, and 20 min, respectively. This represents an improvement of approximately 52%, 68%, 59%, and 56% compared to the unreinforced AA5754 at the corresponding time intervals. The SiO_2-reinforced composite exhibited the second-best performance, followed by the Al_2O_3-reinforced composite, which still outperformed the unreinforced material but with a less pronounced effect than the other reinforcements. The two-pass FSPed samples (Figure 10) exhibited an overall reduction in the specific wear rates across all materials compared with their single-pass counterparts. This improvement can be attributed to the enhanced distribution of reinforcement particles and the more refined microstructure achieved through the additional FSP pass. The hierarchy of wear resistance remained consistent, with the CNTS-reinforced composite exhibiting the lowest specific wear rate of 3.1×10^{-4}, 1.8×10^{-4}, 2.0×10^{-4}, and 1.5×10^{-4} $mm^3/N\cdot m$ at 5, 10, 15, and 20 min, respectively, followed by the SiO_2 and Al_2O_3 reinforce The enhancement in wear resistance for the CNTS-reinforced composite compared to the unreinforced material after two passes reached approximately 66%, 50%, 33%, and 46% at 5, 10, 15, and 20 min, respectively. A notable observation from both Figures 9 and 10 is the declining trend of the specific wear rate with increasing test duration for all materials. The unreinforced AA5754 exhibited the most significant initial wear rate of 1.0×10^{-3} $mm^3/N\cdot m$ at 5 min for single-pass FSP, which gradually decreased to 4.5×10^{-4} $mm^3/N\cdot m$ at 20 min. This pronounced reduction (approximately 55%) indicates that the base material underwent substantial surface modification during the initial stages of wear, forming a work-hardened layer that provided some protection against further wear. In contrast, the CNTS-reinforced composite exhibited a more stable wear behavior with less dramatic reductions in the wear rate over time (approximately 58% reduction from 5 to 20 min for the single-pass FSP and 52% for the two-pass FSP). This suggests that CNTS reinforcement provides immediate protection against wear, thereby reducing the severity of the initial running-in period. Comparing Figures 9 and 10, it is evident that increasing the number of FSP passes from one to two significantly improved the wear resistance of all materials. The reduction in the specific wear rate for the two-pass samples compared to the single-pass samples at 5 min of testing was approximately 35%, 30%, 20%, and 10% for the CNTs-, SiO_2-, Al_2O_3-reinforced, and unreinforced AA5754, respectively. This enhancement can be attributed to the second FSP pass, which further broke down the agglomerates and promoted a homogeneous distribution of the reinforcement in the Al matrix. Furthermore, multiple FSP passes led to additional grain refinement and the elimination of defects, such as micro tunnels, as observed in the macrostructural analysis (Figure 5). In addition, the increased hardness resulting from the second FSP pass (Figure 8) contributed to improved wear resistance.

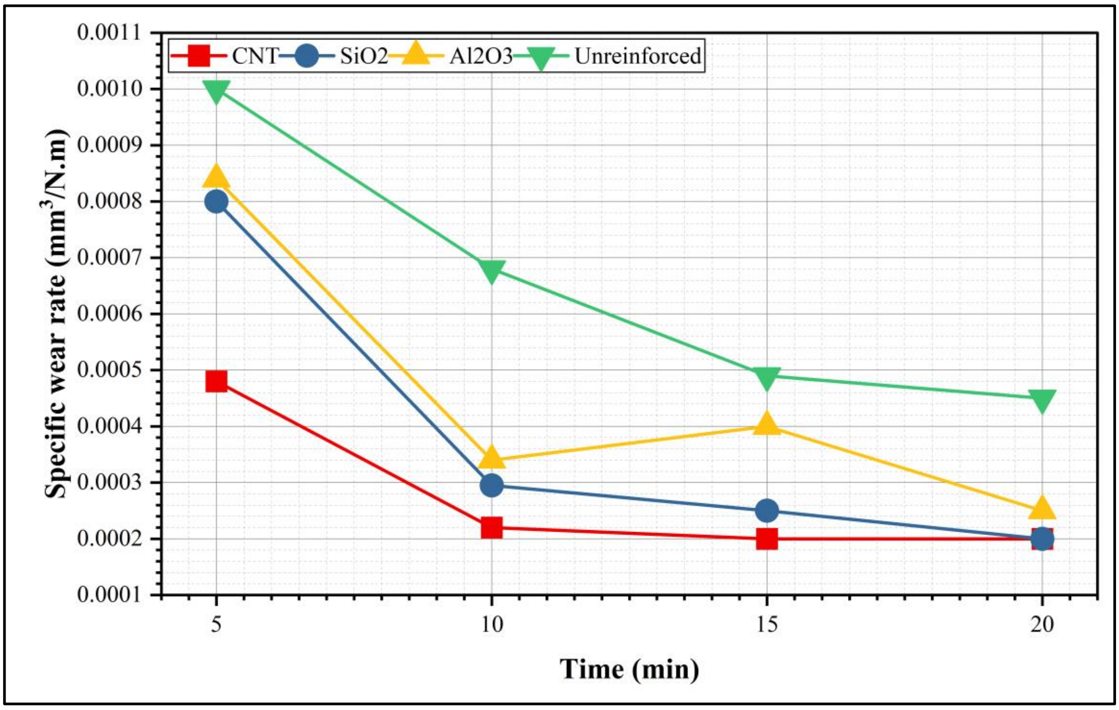

Fig. 9: Specific wear rate of the AA5457 FSPed samples processed using one pass.

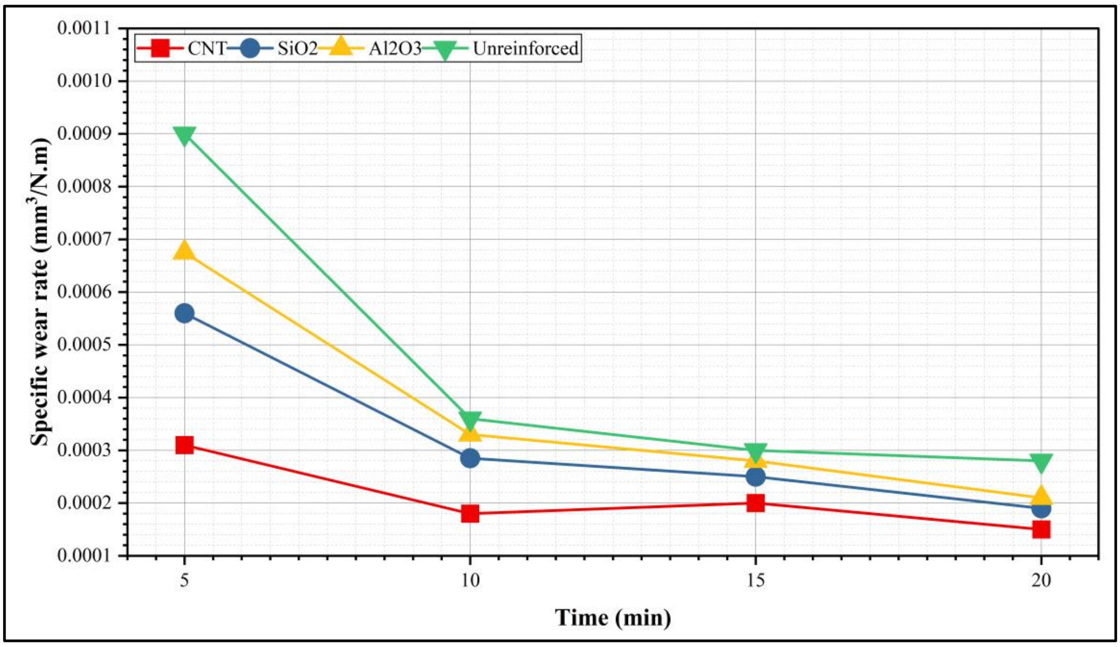

Fig. 10: Specific wear rate of the AA5457 FSPed samples processed using two passes.

Figure 11 presents the friction coefficient data for the AA5754 FSPed samples reinforced with different nano powders of CNTs, SiO_2, and Al_2O_3 processed using one and two passes. The friction coefficient values demonstrated a clear hierarchy among the tested materials. The as-received AA5754 base material exhibited the highest friction coefficient of 0.68894, indicating poor tribological performance. All FSP-processed samples showed reduced friction coefficients compared to the base material, with the following order of increasing friction coefficient: AA5754/CNTs $<$ AA5754/SiO_2 $<$ AA5754/Al_2O_3 $<$ unreinforced AA5754. The CNTS-reinforced composite exhibited the lowest friction coefficient values of 0.49844 and 0.47765 for one and two passes, respectively. This represents approximately 27.7% and 30.7% reduction in the friction coefficient compared to the base material. The superior tribological performance of the CNT-reinforced composite can be attributed to the unique lubrication mechanism of the CNTs. CNTs can form a protective tribofilm on the sliding surface, which reduces direct metal-to-metal contact and consequently decreases frictional forces during sliding wear. The SiO_2-reinforced composite exhibited intermediate friction coefficient values of 0.53813 and 0.51583 for one and two passes, respectively, representing approximately 21.9% and 25.1% reductions compared to the base material. Meanwhile, the Al_2O_3-reinforced composite demonstrated friction coefficient values of 0.58084 and 0.55552, corresponding to reductions of 15.7% and 19.4% compared to the base material. The unreinforced AA5754 processed by FSP also showed improved friction coefficient values of 0.62903 and 0.61656 for one and two passes, respectively, representing approximately 8.7% and 10.5% reductions, respectively, compared to the as-received material. This improvement can be attributed to the microstructural refinement achieved through FSP, even without the addition of reinforcement. Another significant finding was the consistent improvement in the friction coefficient with an increasing number of FSP passes across all material compositions. The two-pass processed samples exhibited lower friction coefficients than their single-pass counterparts, with reductions of approximately 4.2%, 4.1%, 4.4%, and 2.0% for CNTs-, SiO_2-, and Al_2O_3-reinforced and unreinforced AA5754 samples, respectively. This improvement can be attributed to the enhanced distribution of the reinforcement particles and further refinement of the microstructure achieved through the second FSP pass. The second pass effectively reduced particle agglomeration and improved the interfacial bonding between the reinforcements and Al matrix and created a more homogeneous composite structure. These factors collectively contribute to a more stable and uniform tribological response during the wear testing. The results aligned with previous study by Al-Qutub et al. [28] investigated the machinability of Al6061 composites reinforced with CNTs fabricated using spark plasma sintering. They reported that the addition of CNTs led to a reduction in cutting forces and improved surface finish during machining. This improvement was attributed to the solid lubrication effect of CNTs, which reduced the friction at the tool-workpiece interface. Although the study primarily focused on machinability, the observed reduction in cutting forces and improved surface finish suggest potential enhancements in wear resistance and friction behavior due to the presence of CNTs in the Al matrix. Furthermore, Abdeltawab et al. [29] found that the CNTs-reinforced Al composite exhibited a lower wear rate and friction coefficient. This improvement was attributed to the solid lubrication effect of CNTs and their ability to bear load, reducing direct metal-to-metal contact. In addition, Bharti et al. [30] examined the micro-hardness and wear behavior of AA2014 Al alloy surface composites reinforced with Al_2O_3 particles using FSP. They utilized FSP to incorporate Al_2O_3 particles into an AA2014 alloy matrix. Two rotational speeds, 1000 rpm and 1400 rpm, were employed to assess their effect on the microstructure and wear properties. They reported that the incorporation of Al_2O_3 particles led to a significant reduction in grain size and an increase in microhardness by approximately 30% compared to that of the base material. The wear tests revealed that both the wear performance and friction coefficient improved after FSP. The friction coefficient decreased from 0.27461 in the base material to 0.22570 in the FSPed samples. The enhanced wear resistance and reduced COF were attributed to the uniform distribution of hard Al_2O_3 particles, which acted as barriers to material removal during sliding. Regarding the effect of the number of FSP passes, studies have shown that increasing the number of passes can lead to a more homogeneous microstructure and improved mechanical properties [31,32]. For instance, a study on Al-5052/SiC composites revealed that multiple FSP passes enhanced properties such as hardness and wear resistance due to better dispersion of reinforcement particles and refined grain structures [1,33]. Similarly, research on AA6060-T4 alloy matrix composites indicated that additional FSP passes contributed to microstructural homogenization, resulting in improved mechanical properties and wear resistance [34].

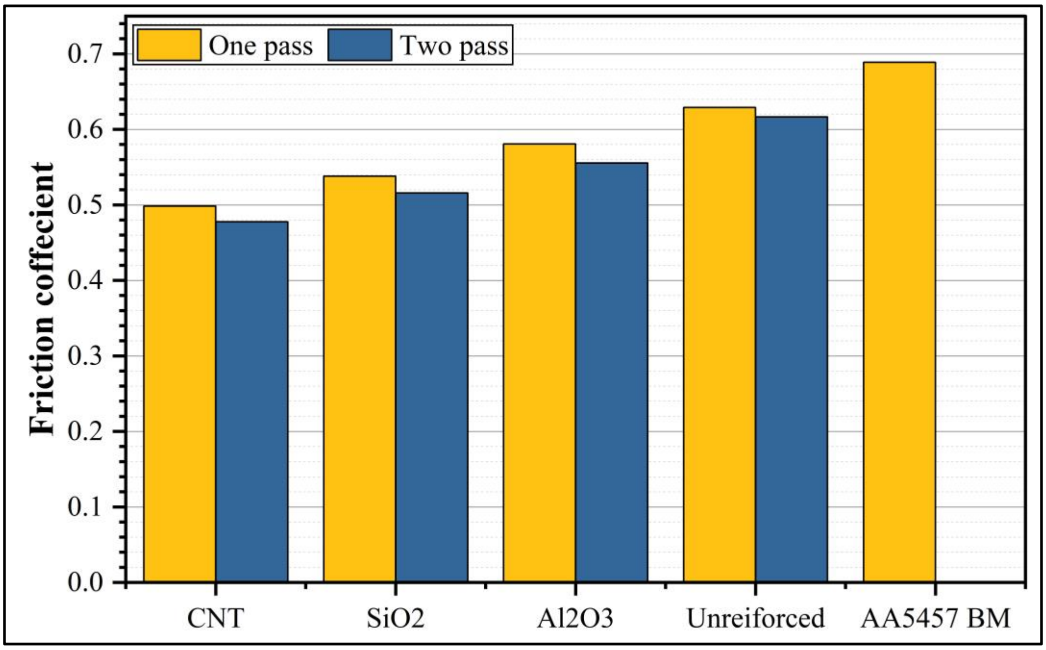

Fig. 11: Friction coefficient of the AA5457 FSPed samples processed using one and two passes.

3.3.2. Wear Mechanisms of FSPed Composites

For the unreinforced AA5754 samples (Figures 12a,b, and 13a), the worn surfaces exhibited severe wear characteristics after both single and double-pass FSP. The single-pass sample exhibited deep wear tracks, extensive plastic deformation, and large areas of delamination. This indicates that the predominant wear mechanism was adhesive wear coupled with severe plastic deformation. The presence of detached debris particles suggests material removal through a combination of adhesive and abrasion wear processes. After two FSP passes (Figure 13a), although the wear track depth appeared to decrease slightly, there was still evidence of significant material removal and plastic deformation. The presence of accumulated debris and microcracks on the worn surface indicates that the wear resistance improved marginally with the second FSP pass, likely owing to grain refinement; however, the material still experienced considerable wear [35,36]. The CNTs-reinforced composite (Figures 12c and d and 13b) demonstrated the most significant improvement in wear resistance among all the tested materials. After a single FSP pass (Figure 12c,d), the worn surface exhibited shallow wear tracks with minimal plastic deformation and debris. This suggests that the CNTs effectively enhanced the load-bearing capacity of the Al matrix and provided a solid-lubrication mechanism. The two-pass FSPed CNTs composite (Figure 13b) showed further improvement, with shallower wear tracks and finer debris particles. The formation of a thin, deformed layer on the surface indicates the development of a stable tribofilm, which is characteristic of CNTs-reinforced composite. This tribofilm acts as a protective barrier, reducing direct metal-to-metal contact and consequently decreasing wear. The SiO_2-reinforced composite (Figures 12e,f and 13c) exhibited an intermediate wear performance between the unreinforced AA5754 and CNTs-reinforced composite. After a single FSP pass (Figure 12e,f), the worn surface displayed shallow wear tracks with some evidence of microabrasion and plastic deformation. The presence of microcracks on the worn surface of SiO_2-reinforced composites indicates the development of localized stress concentrations during the wear process. These stress concentrations can be attributed to several interrelated factors; despite the FSP process, some regions exhibited non-uniform distribution of SiO_2 particles, creating areas with particle clustering. These clusters act as stress risers during the wear process, initiating microcracks that propagate along the particle-matrix interfaces. The two-pass FSPed SiO_2 composite (Figure 13c) exhibited improved wear resistance, with shallower wear tracks and reduced debris formation. However, the presence of microcracks, though less pronounced than in the single-pass samples, suggests that the material still experienced some localized stress concentrations. The Al_2O_3-reinforced composite (Figures 12g,h and 13d) demonstrated improved wear resistance compared with the unreinforced AA5754 but was less effective than the CNTs and SiO_2 reinforcements. After a single FSP pass (Figure 12g,h), the worn surface showed deep wear tracks and evidence of severe agglomeration of Al_2O_3 particles. This agglomeration likely led to stress concentration and localized wear, thereby reducing the overall wear resistance. The two-pass FSPed Al_2O_3 composite (Figure 13d) showed significant improvement, with shallower wear tracks and reduced particle agglomeration. This suggests that the second FSP pass was particularly effective in breaking up the Al_2O_3 clusters and achieving a more uniform particle distribution, resulting in enhanced wear resistance. The observed wear mechanisms and surface features, as shown in Figures 12 and 13, correlate well with the wear rate (Figures 9 and 10) and friction coefficient (Figure 11). The CNTs-reinforced composite consistently demonstrated the best wear performance, characterized by shallow wear tracks, fine debris, and the formation of protective tribofilms. This can be attributed to the unique properties of CNTs, including their high strength, excellent thermal conductivity, and ability to form strong interfacial bonds with the Al matrix. The SiO_2 and Al_2O_3 reinforced composites showed intermediate wear performance, with the effectiveness of the reinforcement improving after two FSP passes. This improvement can be attributed to the better particle distribution and matrix refinement achieved through multiple FSP passes. However, the presence of hard ceramic particles also introduced some abrasive wear mechanisms, particularly in the case of Al_2O_3.

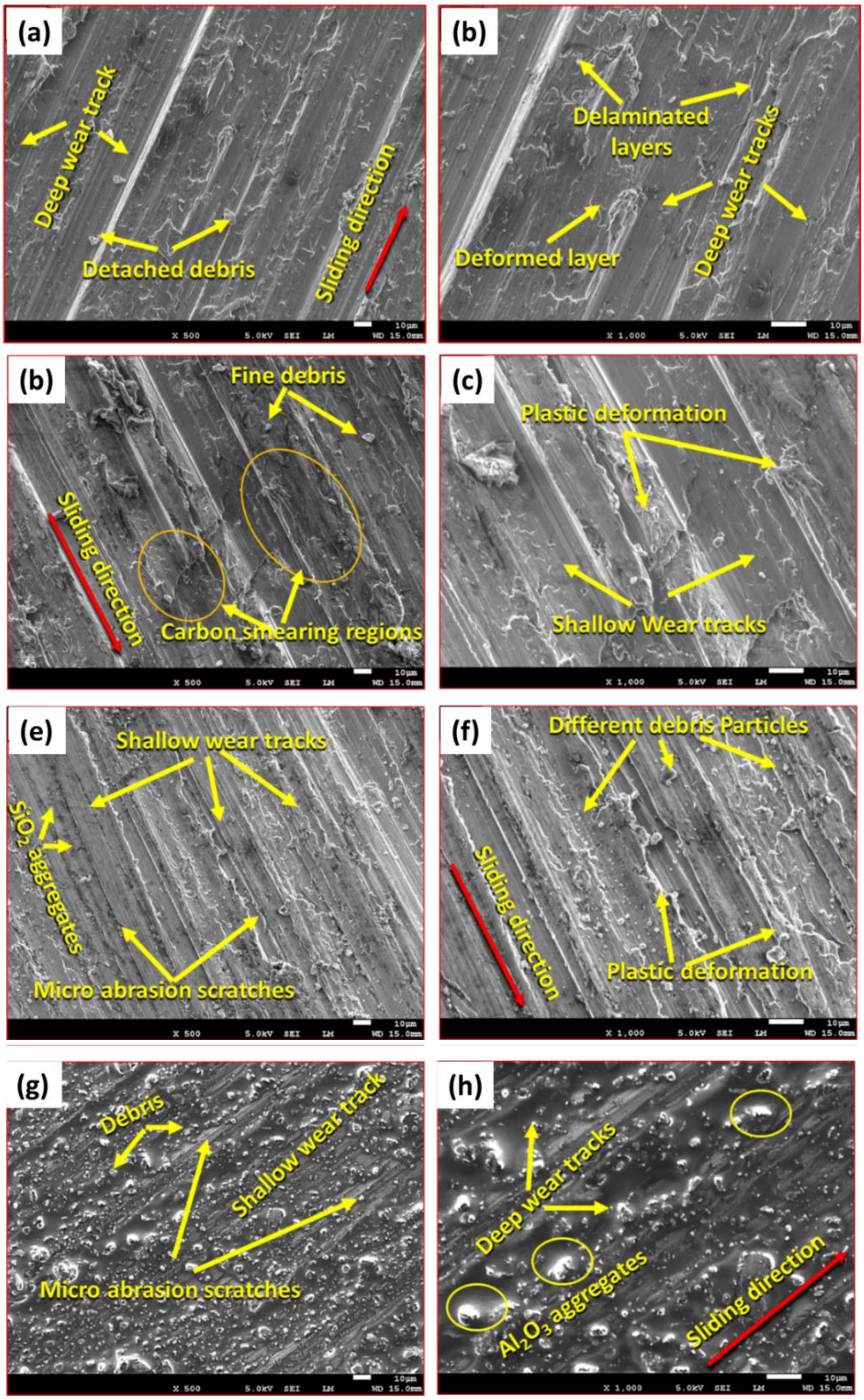

Fig. 12: Worn surfaces of (a,b) unreinforced AA5754, (c,d) AA5754/CNTs, (c,d) AA5754/SiO_2, and (e,f) AA5754/Al_2O_3 FSPed at one pass.

3.3.3. Wear depth of worn surface.

The surface roughness in terms of the wear depth versus the lateral position of the worn surfaces of (a) AA5754 BM, (b) AA5754 Al/CNTs (c) AA5754 Al/SiO_2, and (d) AA5754 Al/Al_2O_3 composites produced using two FSP passes after dry wear testing at 7 N, a speed of 0.4 m/s, and a testing time of 10 min. The surface roughness of all the wear-tested Al alloy and composite specimens exhibited various roughness profiles based on the SEM images of the worn surface, as shown in Figures 13. Figure 14 shows that the composite containing

CNTs exhibited the lowest mean wear depth as a function of the wear track of 0.3956 µm ±0.01337 compared to the composites of AA5754 Al/SiO_2 (0.4087 µm ± 0.01901), AA5754 Al/Al_2O_3 (0.4104 ± 0.02754), and AA5754 BM (0.4542 ± 0.02554). Based on these results, it can be concluded that the mean wear depth of the Al-based composites can be reduced by the addition of reinforcements, such as CNTs, SiO_2, and Al_2O_3, compared to that of the unreinforced alloy. Among these, CNTs-reinforced Al-based composites generally exhibited the most significant reduction in mean wear depth, followed by alumina and silica reinforcements.

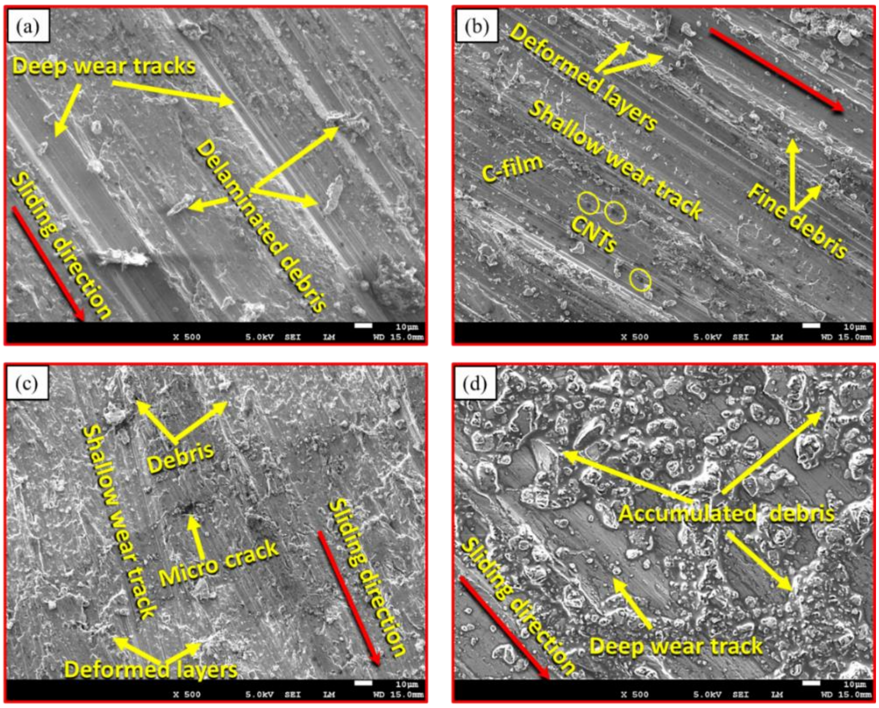

Fig. 13: Worn surfaces of (a,b) unreinforced AA5754, (c,d) AA5754/CNTs, (c,d) AA5754/SiO_2, and (e,f) AA5754/Al_2O_3 FSPed at two passes.

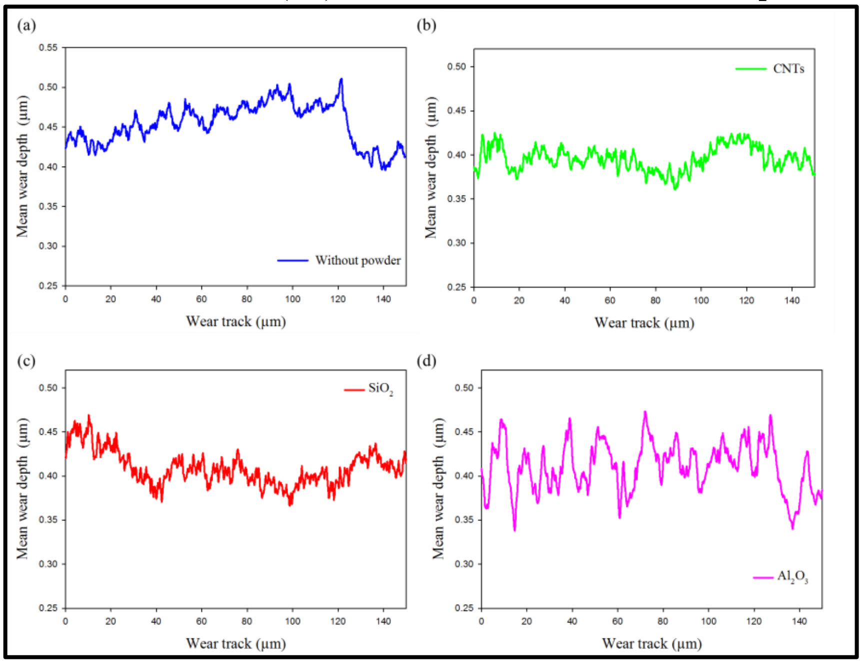

Fig. 14: Mean wear depth against the wear track of the worn surfaces of (a) AA5754 BM, (b) AA5754/CNTs (c) AA5754/SiO_2, and (d) AA5754/Al_2O_3 produced using two passes.

3.3.4. Bearing area analysis

The bearing area analysis, also known as the Abbott-Firestone curve, provides an understanding of the surface topography characteristics of the worn surfaces of wear-tested specimens. Figures 15, 16, 17, and 18 present the bearing area curves for AA5754 BM, AA5754/CNTs, AA5754/SiO_2, and AA5754/Al_2O_3 composites, respectively, produced using two FSP passes after wear testing. It can be remarked that the key surface topography parameters of Rk, Rpk, Rvk, Mr1, and Mr2 derived from these curves reveal significant differences in the tribological behavior of the various nanocomposites. The core roughness depth (Rk) values show a distinctive pattern across the different materials. The AA5754/CNTs composite exhibited the highest Rk value of 0.235 μm compared to 0.22225 μm for the base material, indicating a relatively thicker functional core zone. In contrast, the AA5754/Al_2O_3 composite showed a significantly lower Rk value of 0.05631 μm, suggesting that alumina reinforcement created a more stable and uniform surface layer during the wear process. The AA5754/SiO_2 composite demonstrated an intermediate Rk value of 0.20075 μm, slightly lower than the base material. The reduced peak height (Rpk) parameter, which represents the portion of the surface that will be worn away during the initial running-in period, showed notable variations. The base material exhibited an Rpk value of 0.08456 μm, while the CNTs, SiO_2, and Al_2O_3 reinforced composites displayed values of 0.06398 μm, 0.07026 μm, and 0.0041 μm, respectively. The remarkably low Rpk value for the Al_2O_3-reinforced composite suggests minimal material removal during the initial running-in phase, which correlates with its enhanced wear resistance observed in wear testing results (Section 3.3.1). The CNTs reinforced composite also showed improved Rpk compared to the base material, aligning with its superior tribological performance. The reduced valley depth (Rvk) parameter, which indicates the fluid retention capability of the surface, showed that the CNTs reinforced composite had the highest value of 0.07646 μm compared to 0.06089 μm for the base material. This increased valley depth potentially allows for better lubricant retention in actual service conditions, which could further enhance the tribological performance of CNTs reinforced composites in lubricated applications. The Al_2O_3 and SiO_2 reinforced composites showed Rvk values of 0.05646 μm and 0.06821 μm, respectively. The material ratio parameters (Mr1 and Mr2) also revealed important characteristics of the worn surfaces. The Mr1 values, corresponding to the upper limit of the core roughness, were 0.10346, 0.09106, 0.06317, and 0.04469 for the base material, CNTs, SiO_2, and Al_2O_3 reinforced composites, respectively. The lower Mr1 values for the reinforced composites indicate a smaller proportion of material in the peak region, suggesting more uniform wear characteristics. Similarly, the Mr2 values, representing the lower limit of the core roughness, were 0.93752, 0.91442, 0.88873, and 0.89339 for the base material, CNTs, SiO_2, and Al_2O_3 reinforced composites, respectively. The slightly lower Mr2 values for the reinforced composites suggest more effective valley structures that could potentially enhance debris entrapment and wear resistance. These bearing area analysis results correlate well with the observed wear mechanisms discussed in Section 3.3.2 and surface roughness analysis in Section 3.3.3. The CNTs reinforced composite, which demonstrated the best overall wear resistance, showed a favorable combination of relatively low Rpk (minimizing initial material removal) and high Rvk (enhancing potential lubricant retention). The unique surface characteristics of the CNTs reinforced composite can be attributed to the formation of a protective tribofilm during wear, as evidenced by the SEM observations (Figure 13b). This tribofilm effectively reduces direct metal-to-metal contact and facilitates more controlled and uniform wear. It can be concluded that the bearing area analysis results further support the conclusion that nano reinforcements, particularly CNTs, effectively modify the surface topography during wear, creating more favorable tribological interfaces with enhanced wear resistance and potentially better lubricant retention capabilities compared to the unreinforced AA5754 alloy.

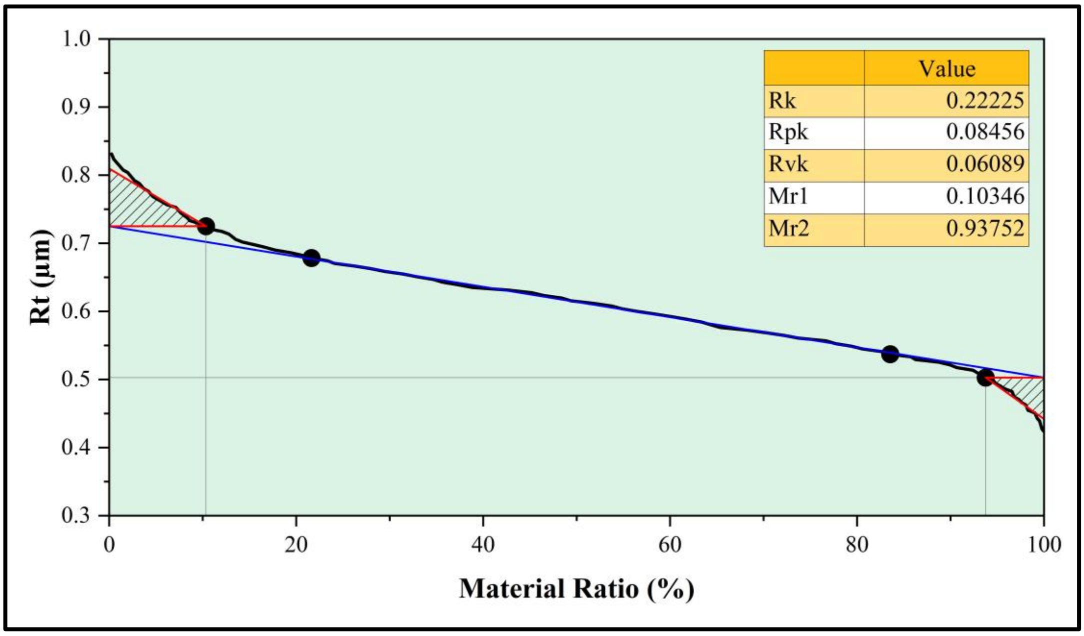

Fig. 15: Bearing area analysis of worn surface of AA5754 BM wear tested sample.

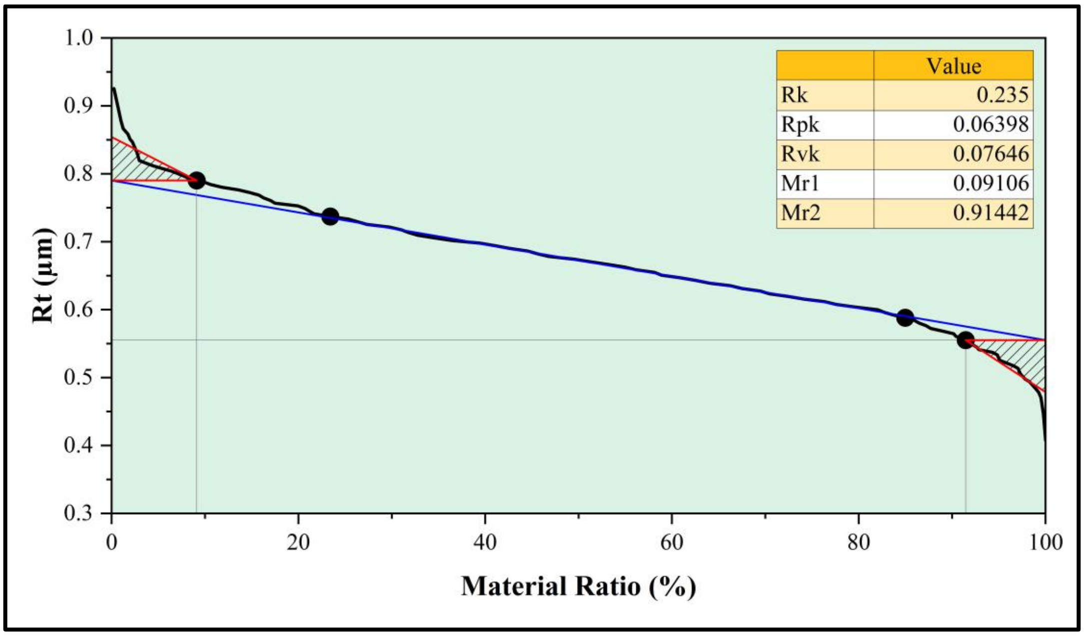

Fig. 16: Bearing area analysis of worn surface of AA5754/CNTs wear tested sample.

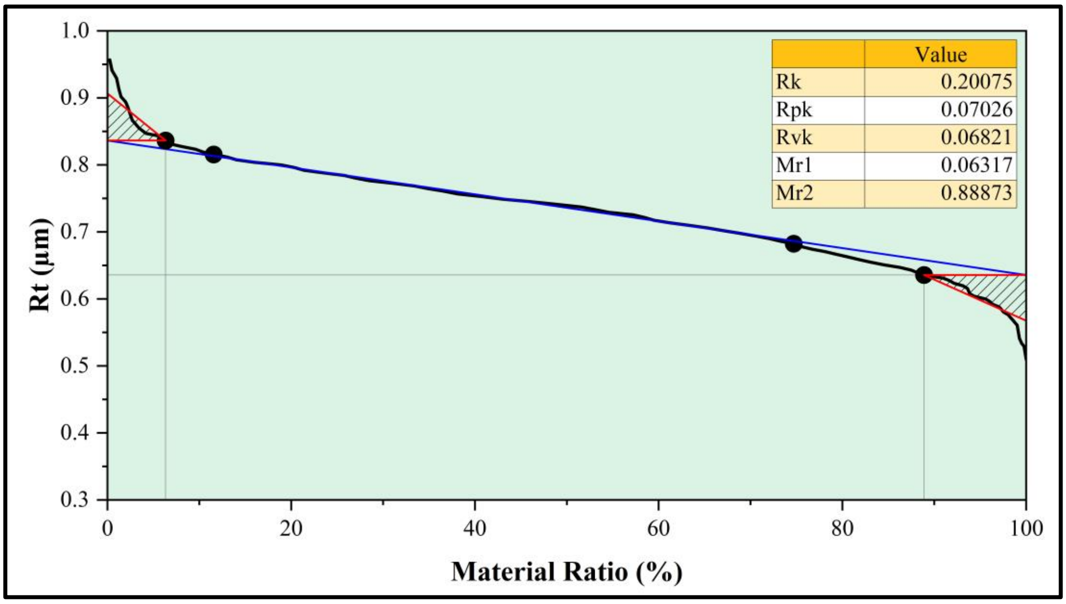

Fig. 17: Bearing area analysis of worn surface of AA5754/SiO_2 wear tested sample.

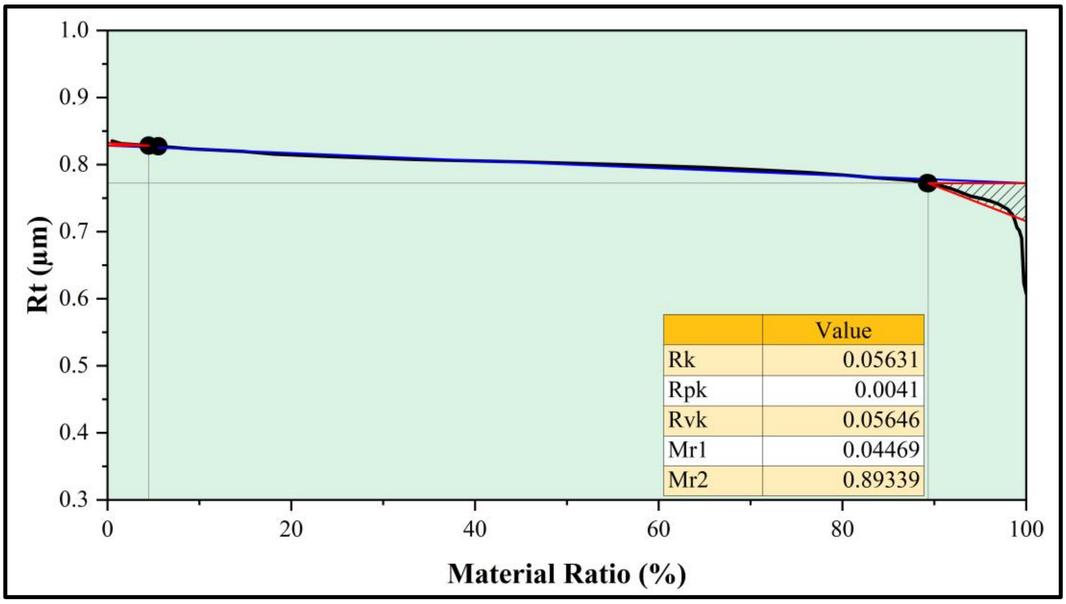

Fig. 18: Bearing area analysis of worn surface of AA5754/Al_2O_3 wear tested sample.

4. Conclusions

In this study, AA5754-based metal matrix nanocomposites reinforced with three distinct nano powders of CNTs, SiO_2, and Al_2O_3 were successfully fabricated via FSP using single and double passes. The following key conclusions were drawn:

1. The incorporation of CNTs, SiO_2, and Al_2O_3 nano powders into the AA5754 aluminum matrix was successfully achieved using a blind hole strategy at a rotational speed of 1660 rpm and a traverse speed of 20 mm/min.
2. All three non-reinforcements enhanced the microhardness of the AA5754 composites, with CNTs-reinforced specimens exhibiting the most substantial improvement after both single and double FSP passes. This enhancement can be attributed to the exceptional load-

bearing capacity of CNTs and their ability to impede dislocation movement within the Al matrix.

3. Tribological assessment revealed that the CNT-reinforced composites possessed the lowest specific wear rate and friction coefficient among all tested materials. This superior wear resistance can be attributed to the unique properties of CNTs, which provide enhanced load-bearing capacity, improved thermal and mechanical properties, and an effective solid lubrication mechanism that facilitates more controlled and uniform wear.
4. Quantitative analysis of wear depth profiles confirmed that the nonreinforcement additions reduced the mean wear depth of the AA5754 composites compared with the unreinforced alloy. The CNT-reinforced composites demonstrated the most significant reduction in mean wear depth, followed by the Al_2O_3 and SiO_2 reinforcements.
5. Bearing area analysis showed that nano reinforcement additions, especially CNTs, improved the functional surface topography of AA5754 composites after wear. CNT-reinforced composites exhibited lower peak heights, deeper valleys, and more uniform material ratios, indicating minimized initial material removal, better lubricant retention, and enhanced load-bearing capacity.

5. Future Directions

Based on the findings of this study, several avenues for future research can be identified to further advance the understanding and optimization of FSP AA5754 nanocomposites reinforced with CNTs, SiO_2, and Al_2O_3.

1. Apply XRD and EDS mapping after SEM imaging to conclusively identify the phases present, confirm the retention of reinforcement particles, and verify the chemical composition of both the matrix and the reinforcements.
2. Explore alternative powder incorporation techniques, such as groove filling, surface pre-coating, or interlayer strip.
3. The effects of FSP parameters, such as rotation speed, traverse speed, and number of passes, were explored, and different tool pin geometries, such as triangular, square, tapered, and cylindrical, were compared to optimize the material flow, reinforcement dispersion, and defect elimination for each nano powder type.
4. Quantitative grain size measurements in the SZ, TMAZ, and HAZ are included to provide a comprehensive understanding of the microstructural evolution and its impact on the composite performance.

Acknowledgment

This study is supported via funding from Prince Sattam bin Abdulaziz University project number (PSAU/2025/R/1446)

References

[1] Abdullah ME, Mohammed MM, Ahmed FS, Kubit A, Aghajani Derazkola H. Evaluating the microstructural and mechanical properties of TiO2/AA7075 metal matrix nanocomposite via

friction stir processing. International Journal of Advanced Manufacturing Technology 2025;137:4741–60. https://doi.org/10.1007/S00170-025-15437-7/FIGURES/17.

[2] Rohim MNM, Abdullah ME, Mohammed MM, Kubit A, Aghajani Derazkola H. Friction Stir Processed AA5754-Al2O3 Nanocomposite: A Study on Tribological Characteristics. Journal of Composites Science 2024, Vol 8, Page 216 2024;8:216. https://doi.org/10.3390/JCS8060216.

[3] Abdullah ME, M. Rohim MN, Mohammed MM, Derazkola HA. Effects of Partial-Contact Tool Tilt Angle on Friction Stir Welded AA1050 Aluminium Joint Properties. Materials 2023, Vol 16, Page 4091 2023;16:4091. https://doi.org/10.3390/MA16114091.

[4] Mishra A, Tiwari A, Shukla MK, Rose AR. Analysis of Tools used in Friction Stir Welding process. International Journal of Current Engineering and Technology 2018;8. https://doi.org/10.14741/ijcet/v.8.6.2.

[5] Abdullah ME, M. Rohim MN, Mohammed MM, Derazkola HA. Effects of Partial-Contact Tool Tilt Angle on Friction Stir Welded AA1050 Aluminium Joint Properties. Materials 2023, Vol 16, Page 4091 2023;16:4091. https://doi.org/10.3390/MA16114091.

[6] Mohammed MM, Abdullah ME, Rohim MNM, Kubit A, Derazkola HA. AA5754–Al2O3 Nanocomposite Prepared by Friction Stir Processing: Microstructural Evolution and Mechanical Performance. Journal of Manufacturing and Materials Processing 2024, Vol 8, Page 58 2024;8:58. https://doi.org/10.3390/JMMP8020058.

[7] Habba MIA, Ahmed MMZ. Friction stir welding of dissimilar aluminium and copper alloys: A review of strategies for enhancing joint quality. Journal of Advanced Joining Processes 2025;11. https://doi.org/10.1016/j.jajp.2025.100293.

[8] Samal P, Vundavilli PR, Meher A, Mahapatra MM. Recent progress in aluminium metal matrix composites: A review on processing, mechanical and wear properties. J Manuf Process 2020;59:131–52. https://doi.org/10.1016/j.jmapro.2020.09.010.

[9] Mishra RS, Ma ZY, Charit I. Friction stir processing: A novel technique for fabrication of surface composite. Materials Science and Engineering: A 2003;341:307–10. https://doi.org/10.1016/S0921-5093(02)00199-5.

[10] Yang J song, Luo Z an, Zhang X, Wang M kun, Liu Z song, Xie G ming, et al. Through-thickness particle distribution, microstructure evolution and tribological performance of B4C/BN-AA6061 composite via friction stir processing. Wear 2024;558–559. https://doi.org/10.1016/j.wear.2024.205555.

[11] Sangamaeswaran R, Muhilan S, Navin J, Austin Manuelraj P, Palaniappan M. Mechanical and wear properties of friction stir processing AA 6082-T6/B4C aluminium matrix composites. Mater Today Proc 2023:4–9. https://doi.org/10.1016/j.matpr.2023.05.112.

[12] Ahmed MMZ, El-Sayed Seleman MM, Fydrych D, Çam G. Review on Friction Stir Welding of Dissimilar Magnesium and Aluminium Alloys: Scientometric Analysis and Strategies for Achieving High-Quality Joints. Journal of Magnesium and Alloys 2023;Accepted. https://doi.org/https://doi.org/10.1016/j.jma.2023.09.039.

[13] Alidokht SA, Abdollah-zadeh A, Soleymani S, Assadi H. Microstructure and tribological performance of an aluminium alloy-based hybrid composite produced by friction stir processing. Mater Des 2011;32:2727–33. https://doi.org/10.1016/j.matdes.2011.01.021.

[14] Rana HG, Badheka VJ, Kumar A. Fabrication of Al7075 / B4C Surface Composite by Novel Friction Stir Processing (FSP) and Investigation on Wear Properties. Procedia Technology 2016;23:519–28. https://doi.org/10.1016/j.protcy.2016.03.058.

[15] Srinivasan C, Karunanithi M. Fabrication of surface level Cu/SiCp nanocomposites by friction stir processing route. J Nanotechnol 2015;2015. https://doi.org/10.1155/2015/612617.

[16] Reddy G, Rao A, Rao K. Friction Stir Surfacing Route: Effective Strategy for the Enhancement of Wear Resistance of Titanium Alloy. Transactions of the Indian Institute of Metals 2013;66. https://doi.org/10.1007/s12666-013-0254-x.

[17] Bauri R, Yadav D, Shyam Kumar CN, Balaji B. Tungsten particle reinforced Al 5083 composite with high strength and ductility. Materials Science and Engineering: A 2015;620:67–75. https://doi.org/10.1016/j.msea.2014.09.108.

[18] Sharifitabar M, Sarani A, Khorshahian S, Shafiee Afarani M. Fabrication of 5052Al/Al2O3 nanoceramic particle reinforced composite via friction stir processing route. Mater Des 2011;32:4164–72. https://doi.org/10.1016/j.matdes.2011.04.048.

[19] Shafiei-Zarghani A, Kashani-Bozorg SF, Zarei-Hanzaki A. Microstructures and mechanical properties of Al/Al2O3 surface nano-composite layer produced by friction stir processing. Materials Science and Engineering: A 2009;500:84–91. https://doi.org/10.1016/j.msea.2008.09.064.

[20] Wang W, Shi Q yu, Liu P, Li H ke, Li T. A novel way to produce bulk SiCp reinforced aluminium metal matrix composites by friction stir processing. J Mater Process Technol 2009;209:2099–103. https://doi.org/10.1016/j.jmatprotec.2008.05.001.

[21] Ke L, Huang C, Xing L, Huang K. Al-Ni intermetallic composites produced in situ by Friction Stir Processing. J Alloys Compd 2010 ;503 :494–9. https://doi.org/10.1016/j.jallcom.2010.05.040.

[22] Cui GR, Ni DR, Ma ZY, Li SX. Effects of Friction Stir Processing Parameters and In Situ Passes on Microstructure and Tensile Properties of Al-Si-Mg Casting. Metall Mater Trans A Phys Metall Mater Sci 2014;45:5318–31. https://doi.org/10.1007/s11661-014-2494-8.

[23] El-Rayes MM, El-Danaf EA. The influence of multi-pass friction stir processing on the microstructural and mechanical properties of Aluminium Alloy 6082. J Mater Process Technol 2012;212:1157–68. https://doi.org/10.1016/j.jmatprotec.2011.12.017.

[24] Yang R, Zhang Z, Zhao Y, Chen G, Guo Y, Liu M, et al. Effect of multi-pass friction stir processing on microstructure and mechanical properties of Al3Ti/A356 composites. Mater Charact 2015;106:62–9. https://doi.org/10.1016/j.matchar.2015.05.019.

[25] Ostovan F, Amanollah S, Toozandehjani M, Shafiei E. Fabrication of Al5083 surface hybrid nanocomposite reinforced by CNTs and Al2O3 nanoparticles using friction stir processing. J Compos Mater 2020;54:1107–17. https://doi.org/10.1177/0021998319874849.

[26] Mirjavadi SS, Alipour M, Hamouda AMS, Matin A, Kord S, Afshari BM, et al. Effect of multi-pass friction stir processing on the microstructure, mechanical and wear properties of AA5083/ZrO2 nanocomposites. J Alloys Compd 2017;726:1262–73. https://doi.org/10.1016/J.JALLCOM.2017.08.084.

[27] ELSayed EM, Ahmed MMZ, Seleman MMEls, EL-Nikhaily AE. Effect of Number of Friction Stir Processing Passes on Mechanical Properties of SiO2/5083Al Metal Matrix Nano-Composite. Journal of Petroleum and Mining Engineering 2017;19:10–7. https://doi.org/10.21608/JPME.2017.38325.

[28] Al-Qutub AM, Khalil A, Saheb N, Hakeem AS. Wear and friction behavior of Al6061 alloy reinforced with carbon nanotubes. Wear 2013;297:752–61. https://doi.org/10.1016/J.WEAR.2012.10.006.

[29] Abdeltawab NM, Esawi AMK, Wifi A. Investigation of the Wear Behavior of Dual-Matrix Aluminium–(Aluminium–Carbon Nanotube) Composites. Metals 2023, Vol 13, Page 1167 2023;13:1167. https://doi.org/10.3390/MET13071167.

[30] Bharti S, Ghetiya ND, Patel KM. Micro-hardness and wear behavior of AA2014/Al2O3 surface composite produced by friction stir processing. SN Appl Sci 2020;2:1–16. https://doi.org/10.1007/S42452-020-03585-2/FIGURES/13.

[31] Luo J, Liu S, Paidar M, Vignesh RV, Mehrez S. Enhanced mechanical and tribological properties of AA6061/CeO2 composite fabricated by friction stir processing. Mater Lett 2022;318:132210. https://doi.org/10.1016/J.MATLET.2022.132210.

[32] Wang Y, Paidar M, Eslami-Farsani R, Ahmadi-Danesh-Ashtiani H, Salman S, Mehrez S, et al. Friction surfacing of AA6061 on AA5083 aluminium alloy with adding 316 stainless steel powders: Effect of volume fraction of reinforcements. Journal of Materials Research and Technology 2024;30:1800–5. https://doi.org/10.1016/J.JMRT.2024.03.066.

[33] Nabi S, Rathee S, Wani MF, Srivastava M. Effect of multiple passes on the properties of Al-5052/SiC surface composites fabricated via friction stir processing. Mater Chem Phys 2024;314:128819. https://doi.org/10.1016/J.MATCHEMPHYS.2023.128819.

[34] Leszczyńska-Madej B, Madej M, Wąsik A, Węglowska A. Microstructural homogenization and mechanical enhancement of aluminium matrix composites via multi-pass friction stir processing with SiC reinforcements. International Journal of Advanced Manufacturing Technology 2024;134:2035–50. https://doi.org/10.1007/S00170-024-14252-W/FIGURES/15.

[35] Moradi Faradonbeh A, Shamanian M, Edris H, Paidar M, Bozkurt Y. Friction Stir Welding of Al-B4C Composite Fabricated by Accumulative Roll Bonding: Evaluation of Microstructure and Mechanical Behavior. J Mater Eng Perform 2018;27:835–46. https://doi.org/10.1007/S11665-018-3131-2/FIGURES/17.

[36] Parizi MT, Ebrahimi GR, Ezatpour HR, Paidar M. The structure effect of carbonaceous reinforcement on the microstructural characterization and mechanical behavior of AZ80 magnesium alloy. J Alloys Compd 2019;809:151682. https://doi.org/10.1016/J.JALLCOM.2019.151682.